ADVANCED MATERIALS INTERFACES
www.advmatinterfaces.de

Direct Visualization of the Solid Electrolyte Interphase and Its Effects on Silicon Electrochemical Performance

*Mahsa Sina, Judith Alvarado, Hitoshi Shobukawa, Caleb Alexander, Viacheslav Manichev, Leonard Feldman, Torgny Gustafsson, Keith J. Stevenson, and Ying Shirley Meng**

Fluoroethylene carbonate (FEC) as an electrolyte additive can considerably improve the cycling performance of silicon (Si) electrodes in Li-ion batteries. However, the fundamental mechanism for how FEC contributes to solid electrolyte interphase (SEI) morphological changes and chemical composition is not well understood. Here, scanning transmission electron microscopy coupled with electron energy loss spectroscopy gives a comprehensive insight as to how FEC affects the SEI evolution in terms of composition and morphology throughout electrochemical cycling. In the first lithiation cycle, the electrode cycled in ethylene carbonate (EC): diethylene carbonate (DEC) forms a porous uneven SEI composed of mostly Li_2CO_3. However, the electrode cycled in EC/DEC/FEC is covered in a dense and uniform SEI containing mostly LiF. Interestingly, the intrinsic oxide layer (Li_xSiO_y) is not observed at the interface of electrode cycled in EC/DEC/FEC after 1 cycle. This is consistent with fluoride anion formation from the reduction of FEC, which leads to the chemical attack of any silicon-oxide surface passivation layer. Furthermore, surface sensitive helium ion microscopy and X-ray photoelectron spectroscopy techniques give further insights to the SEI composition and morphology in both electrodes cycled with different electrolytes.

1. Introduction

Silicon is regarded as a potential candidate for next generation anode material for lithium ion batteries (LIBs). The high theoretical gravimetric energy density of silicon–lithium is attributed to the alloying reaction that occurs during the lithiation state, resulting in a high specific capacity (3579 mAh g^{-1} for $Li_{15}Si_4$), which is ten times greater than the current commercial graphite anode. However, the material undergoes severe mechanical stress and strain due to the volume expansion (300%), typical for lithium alloying reactions, which leads to active material cracking, pulverization, and contact loss with the current collector. In order to mitigate the mechanical degradation processes, clever nanomaterial design of silicon (i.e., particles, wires, core shell) have proved to accommodate the large volume expansion during lithiation.[1–3] Liu et al. demonstrated that silicon cracking and fracture is dependent on the Si particle size, ultimately, determining that below 150 nm crystalline Si particles can endure the mechanical strain of full lithiation.[4] Moreover, Gu et al. observed a two phase lithiation process resulting in mechanical stability improvement for Si nanoparticles (NP) ranging from 60 to 100 nm in size, validating the critical cracking size.[5] Though researchers have improved the volume expansion and active material contact to the current collector, the Si anode still suffers from electrolyte chemical degradation caused by the formation of an unstable solid electrolyte interphase (SEI). As a result of the continuous volume expansion, the unstable SEI continues to consume and trap lithium ions as well as electrolyte during electrochemical cycling.[6,7] Both the mechanical and chemical degradation of Si causes rapid capacity failure and poor columbic efficiency (CE) during electrochemical cycling. Thus several challenges must be resolved in order to realize the pragmatic application of Si based anodes for LIBs.

Previous work has reduced the SEI effects by: (1) a series of backend coatings; (2), varying binders, and conductive additives; and (3) modifying the traditional carbonate based electrolyte.[8–11] Of these, altering the electrolyte composition by the addition of electrolyte additives has successfully improved the chemical degradation of Si anodes. In particular, the addition

Dr. M. Sina, J. Alvarado, H. Shobukawa, Prof. Y. S. Meng
Department of NanoEngineering
Materials Science and Engineering Program
University of California San Diego
La Jolla, CA 92093, USA
E-mail: shmeng@ucsd.edu
C. Alexander
Department of Chemistry
University of Texas at Austin
Austin, TX 78712, USA
V. Manichev, Prof. L. Feldman, Prof. T. Gustafsson
Department of Physics and Astronomy
Rutgers University
Piscataway, NJ 08854, USA
Prof. K. J. Stevenson
Materials Science & Engineering Program
Texas Materials Institute
Center for Nano- and Molecular Science and Technology
Department of Chemistry
University of Texas at Austin
Austin, TX 78712, USA
Prof. K. J. Stevenson
Skolkovo Institute of Science and Technology
Center for Electrochemical Energy Storage
3 Nobel Street, Moscow 143026, Russia

DOI: 10.1002/admi.201600438

of fluorethylene carbonate (FEC) to conventional 1 M $LiPF_6$ in ethylene carbonate (EC): diethylene carbonate (DEC) electrolyte has successfully improved the cycling stability and CE of various Si anode types. Though many researchers have used FEC, little is known on how it improves the SEI formation and its morphology. In response, a series of recent publications have investigated the SEI formation process using advanced surface characterization techniques. Yet contradicting studies regarding the reduction mechanism of FEC have caused researchers to propose differing accounts, where some studies claim that FEC reduces to vinylene carbonate which then self-polymerizes to form either polycarbonates or a poly(alkene).[3,12] While Balbuena et al. used computational methods to study the decomposition of FEC and demonstrated that the most probable decomposition mechanism for FEC occurs via a ring opening reaction to form F^-, CO_2^{2-}, and $CHOCH_2$. These reduction products can then react further to form LiF, RCOLi, and Li_2CO_3. This work agrees that a possibility to the stabilization of Si·s SEI is due to the substantial formation of LiF in the initial cycle as a result of the fast FEC reduction. Schroder, Alvarado et al. used an amorphous Si thin film to reconcile the differing accounts of the FEC reduction mechanism, composition, and morphology.[7] Their results determined that the electrode cycled in (10 wt%) FEC additive forms SEI components that can help facilitate lithium ion transport through the SEI despite being thicker and denser in structure. Xu et al. used Si NP composite electrode to determine the effect of FEC at different state of charge in the initial cycle and as a function of depth, suggesting that FEC aids the preservation of the electrode by forming a uniform dense SEI improving the cycling performance.[6]

The notion that FEC forms a protective uniform SEI has been speculated and proposed by scanning electron microscopy and transmission electron microscopy (TEM).[1,3,13,14] These studies use bright-field (BF)-TEM images mainly to study the volume changes after cycling, not focusing on surface morphology. Etacheri et al. observed the Si nanowires after 30 cycles using TEM; however, they mainly focused on the volume expansion of the Si nanowires after cycling by BF-TEM images with low spatial resolution and not on the SEI morphology evolution.[3] Nie et al. monitored the Si NP's morphology using TEM and SEI elemental composition by EDX.[15] However, they claimed that the morphology of the SEI changes throughout electrochemical cycling, yet the TEM images do not clearly demonstrate this phenomenon. This is largely because the BF-TEM images are not sensitive to the Z-contrast; therefore, how FEC improves the SEI stability in the initial cycles has been proposed but not well characterized by microscopic techniques. Therefore, more work needs to be done in order to determine how FEC affects the SEI-Si NP interface and electrochemical performance given that the SEI formation is found to be heavily influenced by surface chemistry and surface area. It is hypothesized that the rapid decomposition of FEC forms a uniform conformal coating around Si NPs reducing the rate at which the electrolyte decomposes,[6] preventing the Si NPs from being exposed to the electrolyte after initial lithiation and delithiation. Conversely, the electrodes cycled in a conventional electrolyte (EC/DEC) suffer from a porous heterogeneous SEI. This hypothesis has yet to be observed using proper single particle microscopy techniques; therefore, we aim to validate this hypothesis by coupling annular dark field scanning transmission microscopy imaging (ADF-STEM) with electron energy loss spectroscopy (EELS) to provide comprehensive insights into the SEI morphology evolution and observe its evolution throughout progressive electrochemical cycling.[16] Using Z-contrast ADF-STEM images can display the SEI morphology evolution with high-spatial resolution, while EELS analysis is used to correlate the morphology evolution with the chemistry changes throughout electrochemical cycling. For the first time, we discuss the SEI structural differences in the Si NP composite electrodes cycled with EC/DEC and EC/DEC/FEC (FEC 10 wt%) using scanning transmission electron microscopy (STEM) techniques. Furthermore, the chemical composition of the SEI using a linear scan by EELS can elucidate the chemical composition of the SEI from the bulk of the active material to the surface (SEI-Si NP interface). STEM techniques poses many challenges such as the organic compound's instability under electron beam exposure[17,18] and local area probing which limits the statistical analysis. Therefore, we have taken several measures to overcome these difficult challenges, which will be later discussed in a greater detail. One of which is to use X-ray photoelectron spectroscopy (XPS) and helium ion microscopy (HIM) surface sensitive techniques to further validate the scanning transmission electron microscopy coupled with electron energy loss spectroscopy (STEM/EELS) results to give a macroview of the SEI composition and morphology. Herein, we demonstrate how utilizing a suite of characterization tools can be a powerful approach to obtain critical information of the SEI morphology and chemical composition for Si NP composite electrodes.

2. Results and Discussion

2.1. Electrochemical Results

The discharge capacity and CE of the Si NP composite electrodes cycled with EC/DEC and with EC/DEC/FEC are shown in **Figure 1**. The electrodes were cycled within the potential range of 0.05–1 V at C/20 for the first cycle and at C/10 for prolonged cycling. Under these galvanostatic conditions the Si NP composite transformed into lithium–silicon alloy and the electrolyte decomposed to form SEI. The electrodes were discharged by applying a constant current until the voltage reached 50 mV to avoid the $Li_{22}Si_5$ alloy phase.[19] We determined that the EC/DEC electrolyte reduced at 0.8 V, while the FEC additive reduced at a higher voltage consistent previous work.[6,7] The CE and specific capacity of the electrode cycled with EC/DEC/FEC electrolyte has a slightly lower CE and specific capacity than the electrode cycled with EC/DEC after first cycle, however, the CE improves after prolonged electrochemical cycling. This behavior is most likely due to the reduction of the FEC in the first cycle to form F^- that could react with several components within the SEI such as etching the native oxide layer[20] and also form LiF. The reduction process of FEC also generate Li_2CO_3, along with other organic products, which will be discussed in greater detail later. This is consistent with all previous reports demonstrating that the FEC additive improves the performance of Si anodes after prolonged cycling.[3,6,7,12,21] Thereby, further

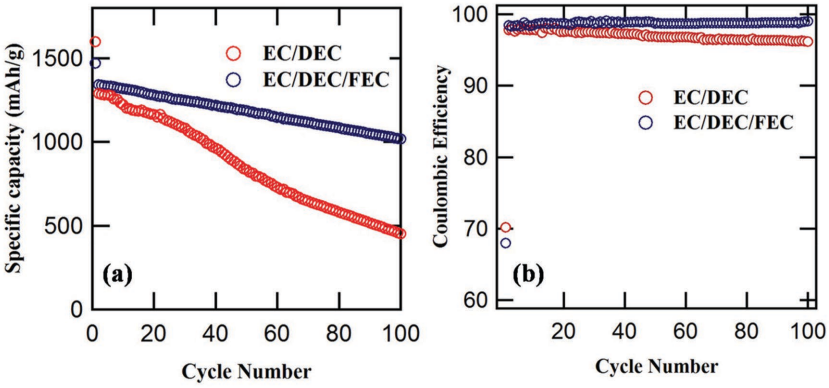

Figure 1. a) Electrochemical cycling performance of Si nanocomposite electrode cycled with EC/DEC and EC/DEC/FEC. b) Coulombic efficiency as a function of cycle number for Si NP with EC/DEC and EC/DEC/FEC.

proving that the FEC reduction stabilizes the Si NP composite interface by forming a rapid uniform coating (compact SEI).

2.2. Surface Characterization

HIM was used for the first time to study the changes in surface morphology of Si NPs after the initial lithiation and 100 electrochemical cycles (delithiated state) at the submicron scale. HIM images of the pristine Si (as casted electrode) and the cycled samples are presented in **Figure 2**. The surface morphology of the pristine particles (Figure 2a) is very smooth and can be easily distinguished. However, it can be clearly seen that the surface morphology changed significantly upon cycling, clearly showing a surface morphology change between the electrode cycled in EC/DEC and EC/DEC/FEC (Figure 2b,c). This is largely due to the difference in electrolyte decomposition products associated with the electrodes in distinct electrolytes. However, Si NPs composite electrode contains inhomogeneity in active surface area and small change in porosity and particle packing can have a large effect on the SEI formation. The surface of the electrode cycled in EC/DEC is rougher than that of the electrode cycled in EC/DC/FEC after 1 cycle. After 100 cycles, both electrodes demonstrated an increase in surface roughness, which can be attributed to the growth of SEI. To further validate the HIM images a combination of characterization techniques such as STEM-EELS and XPS were used to study the morphology and chemistry evolution of SEI throughout electrochemical cycling.

It was found that organic compounds and lithium containing compounds are vulnerable to electron beam exposure because of knock on displacement, radiolysis, and heating effects.[22,23] Conclusively, in this work the electron dose and spatial resolution were optimized during STEM experiments to minimize the electron beam damage to the SEI and Li_xSi compounds. In this regard, the electron beam was spread throughout annular dark field (ADF) imaging and EELS spectra acquisition. The acquisition time was reduced to mitigate the electron dose and prevent beam damage (Figure S1, Supporting Information). Moreover, we lowered the sample temperature to LN_2 temperature to further reduce the beam damage by limiting the diffusion process.[24] The ADF-STEM image of the pristine Si with an average particle size of about 60 nm is shown in Figure S2a in the Supporting Information. The crystalline structure of Si

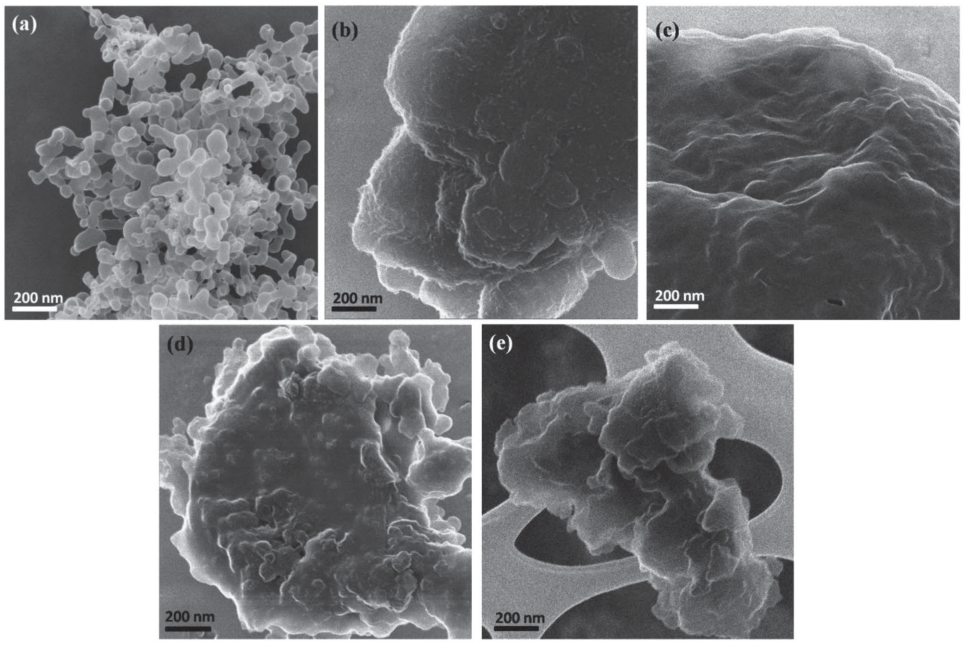

Figure 2. Helium ion microscope images of the a) pristine Si, b) lithiated Si cycled in EC/DEC after 1 cycle, c) lithiated Si cycled in EC/DEC/FEC after 1 cycle, d) delithiated Si cycled in EC/DEC after 100 cycles, and e) delithiated Si cycled in EC/DEC/FEC after 100 cycles.

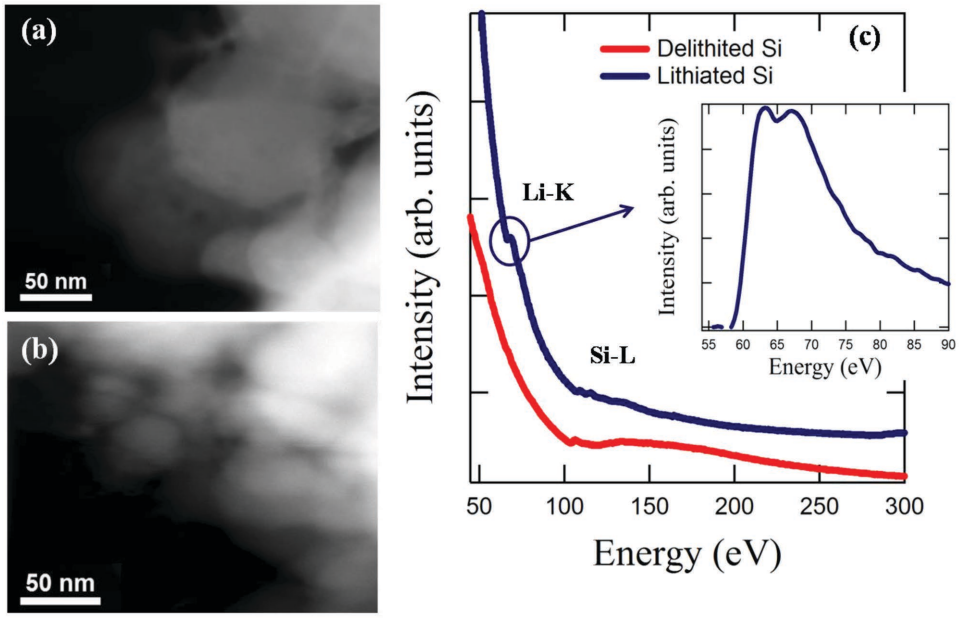

Figure 3. ADF-STEM image of the a) lithiated, b) delithiated Si, and c) EELS spectra of the first lithiated and delithiated Si with EC/DEC. The enlarged Li-K EELS spectrum is shown in the upper right.

can be confirmed from the EELS spectrum (Figure S2b, Supporting Information).[25] As the average particle size of Si is less than 150 nm, the Si NP can withstand the strenuous lithiation process; therefore, in the first few cycles the Si degradation (Figure 1) can largely be attributed to the changes in the surface properties of Si (SEI formation). This allows us to mainly focus on the interfacial chemistry and morphology changes of the cycled Si NP electrodes (SEI) that are associated with the addition of FEC to the traditional electrolyte. The ADF-STEM image of the lithiated Si cycled in EC/DEC is shown in **Figure 3**a. Important changes after lithiation can be observed, especially the expansion of the lithiated crystalline Si particles. EELS spectrum of the lithiated Si (Figure 3c) confirms the formation of amorphous Li_xSi alloys (the enlarged Li-K EELS spectrum is shown in the upper right corner of the Figure 3c).[26] However, after delithiation, the Li-K edge disappears (Figure 3c) suggesting the full delithiation of Si NP. The particle size becomes smaller (Figure 3b) and transforms from crystalline to amorphous Si, which is confirmed by the EELS spectrum (Figure 3c). The regions with low contrast at the edge of the cycled electrodes can be observed in the ADF images (**Figure 4**a,b). This region is ascribed to the presence of the SEI, which is mostly composed of organic compounds (with lower atomic number).[16,27] Based on the STEM images (Figure 4), the electrode cycled with EC/DEC/FEC has an SEI that uniformly coats the entire Si NP in a dense thick film, whereas the electrode cycled with EC/DEC has an inhomogeneous

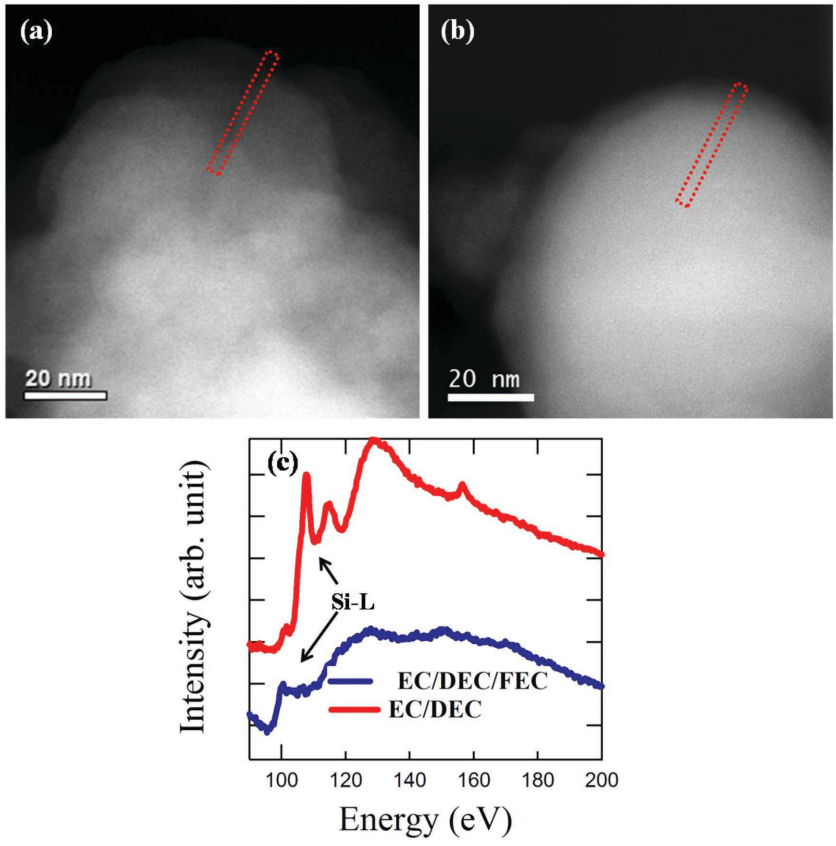

Figure 4. ADF-STEM image of the lithiated Si after 1 cycle cycled in a) EC/DEC, b) EC/DEC/FEC, and c) corresponding EELS spectra from the surface of both electrodes.

porous SEI. Furthermore, EELS scanning profile was performed from the outer surface toward the bulk of these samples (along the indicated line in the Figure 4a,b) to study the chemical changes from the bulk of the particle to SEI. It is worth noting that Si was not detected in the SEI layer for both samples (outer most surface of Si) based on our EELS spectra results, clearly demonstrating that we are solely focusing on characterizing the chemical composition of the SEI. Interestingly, the interfacial chemistry of the lithiated electrode cycled in EC/DEC varied significantly from the electrode cycled in EC/DEC/FEC (Figure 4c), where more lithium silicon oxide alloys are present. The distinct peak shifts toward higher energy for Si-L edge, implies the change in oxidation state of Si.[28] The Si-L fine structure from the surface of the lithiated electrode cycled in EC/DEC/FEC is attributed to amorphous Li_xSi, however, the Si-L fine structure from the surface of the lithiated electrode with EC/DEC corresponds to Li_xSiO_y (Figure 4c).[28] This indicates that the lithiated Si cycled with EC/DEC is covered in a native oxide. These results directly correlate with our previous work, where we propose the reduction mechanism of FEC through a rapid ring opening mechanism, forming fluoride anion.[7] The fluoride anion then undergoes competing reactions to either form HF or LiF (see **Scheme 1**, Equations (1) and (2)). The formation of HF then will etch the native oxide layer causing the formation of less Li_xSiO_y in the electrode cycled with EC/DEC/FEC in the first cycle, which correlate with our previous findings[7,20]

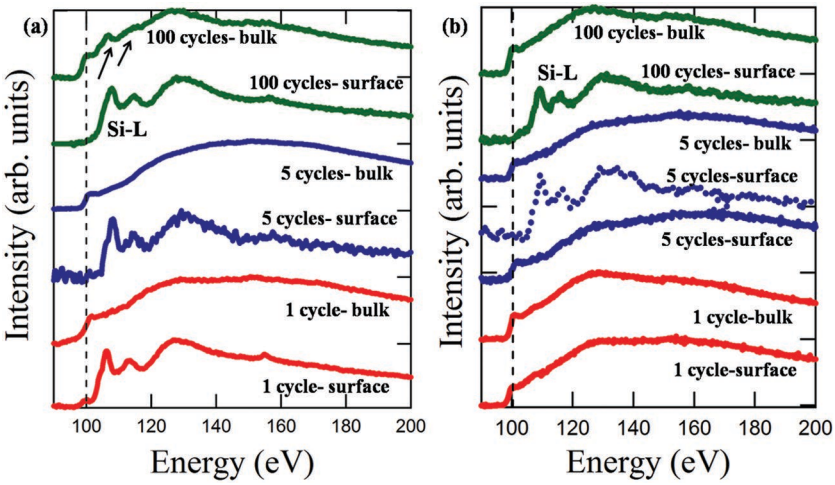

Figure 5. Si-L EELS spectra of the Si electrodes cycled in a) EC/DEC, and b) EC/DEC/FEC after various cycle numbers. The dashed line graph showing the presence of Li_xSiO_y at the surface of the electrode with EC/DEC/FEC after 5 cycles, which is only observed for 2 of the EELS spectra out of 15, acquired EELS spectra.

$$SiO_x + xF^- \rightarrow SiF_x + (x/2)O_2 \quad (1)$$

$$Li^+ + PF_6^- \leftrightarrow PF_5 + LiF \rightarrow LiF + Li_xPF_y \quad (2)$$

$$PF_5 + H_2O_{(trace)} \rightarrow POF_3 + 2HF \quad (3)$$

Thus, the interfacial chemical and morphology evolution between the two electrodes (cycled in EC/DEC and EC/DEC/FEC) can be one of the major factors that lead to electrochemical performance differences. Several researchers have confirmed the existence of silicon oxide layer on the Si electrode, once lithiated its surface (SiO_x) is transformed to Li_xSiO_y which leads to the high impedance and low specific capacity retention.[7,29] It is established that silicon oxide layer has lower flexibility than that of amorphous silicon,[29] consequently, the higher flexibility of the amorphous Li_xSi can endure large volume expansion of silicon upon cycling and maintain the particle integrity. In addition, as the oxide layer on the Si NPs is insulating, it reduces the lithium ion transport and increases the charge transfer impedance, therefore, reducing the cycling properties. This oxide layer consumes Li-ion during lithiation which leads to low specific capacity.[29,7] We further investigated the evolution of Li_xSiO_y and SEI with progressive cycling for the electrodes cycled in EC/DEC and EC/DEC/FEC (1 cycle, 5 cycles, and 100 cycles). Accordingly, we probed the interfacial chemical changes of the electrodes cycled in EC/DEC and EC/DEC/FEC to further understand the role of FEC in oxide layer evolution with cycle number (**Figure 5**). Figure 5a compares the Si-L EELS spectra from surface and bulk of the Si electrodes cycled in EC/DEC after various cycle numbers, where there were no significant changes observed in Si-L edge after progressive cycling. All the Si-L edge taken from the surface of the cycled electrodes in EC/DEC at different cycle numbers correspond to Li_xSiO_y and the Si-L edge from the bulk can be assigned to the Li_xSi. However, the surface and bulk of the Si cycled in EC/DEC/FEC after one cycle corresponding to Li_xSi. After 5 cycles, 2 out of 15 acquired EELS spectra (from various regions) demonstrated the existence of Li_xSiO_y which is shown in dashed line graph in Figure 5b. Meanwhile, the EELS results from the surface of the cycled electrode with EC/DEC/FEC after 100 cycles, only represent the Li_xSiO_y compound. This is most likely due to the, reduction in effects of FEC decomposition compounds as well as an increase in Li_xSiO_y content after 100 cycles. Accordingly, the Si-L edge from the bulk of the electrode cycled in EC/DEC after 100 cycles shows two additional peaks (marked in Figure 5a)

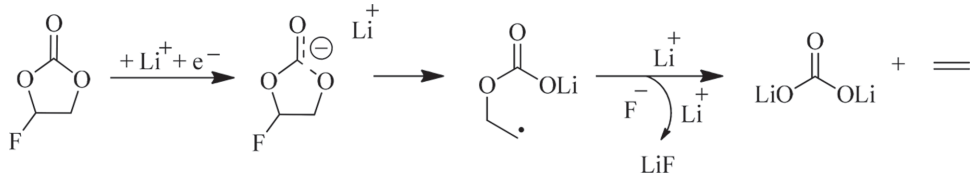

Scheme 1. Electrochemical reduction of FEC via a ring opening mechanism to produce lithium fluoride, lithium carbonate, and ethylene.

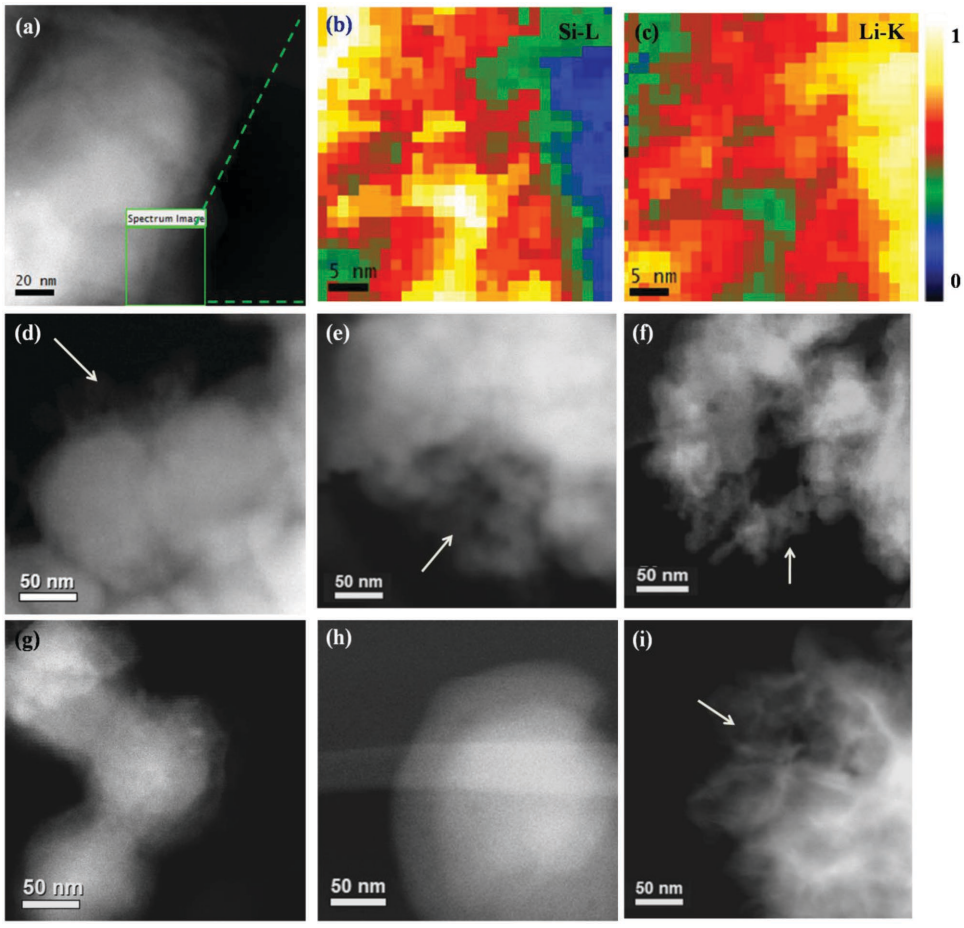

Figure 6. a) ADF-STEM image of the lithiated Si cycled EC/DEC after 1 cycle and the corresponding EELS mapping of b) Si-L, and c) Li-K. ADF-STEM images of the Si electrodes cycled in EC/DEC after d) 1 cycle, e) 5 cycles, f) 100 cycles and the Si electrode cycled in EC/DEC/FEC after, g) 1 cycle, h) 5 cycles, and i) 100 cycles.

corresponding to the infiltration of the native oxide layer (Li_xSiO_y) into the bulk. These results show the increase of native oxide layer with extending cycle number for both electrodes due to further electrolyte reaction with the surface of the electrode. Meanwhile, the diffusion of the oxide layer into the bulk was only found for the electrode cycled in EC/DEC after 100 cycles. This suggests that FEC limits the increase of oxide layer (Li_xSiO_y) with progressive cycling (100 cycles). This may attribute to the improved cycling performance of the electrode cycled in EC/DEC/FEC compared to the electrode cycled in EC/DEC. The increase of Li_xSiO_y was also reported in a recent work indicating that the presence of Li_xSiO_y in high amount for the Si anode (EC/DEC) after 100 cycles lead to capacity fading.[18]

ADF-STEM image (**Figure 6**a) and the corresponding Si-L and Li-K EELS maps were acquired from the lithiated Si samples cycled in EC/DEC (Figure 6b,c) to determine the distribution of Li_xSi and SEI composition. The bright contrast in the image is associated with high Si content; however, the grey regions demonstrate rich Li content in the SEI, which is found on the outer most surface of the particle and further confirms the presence of the SEI. Figure 6d–i shows the ADF-STEM images of SEI with progressive cycling, where the electrode cycled in EC/DEC after the first delithiation forms an inhomogeneous porous SEI. Moreover, this SEI is intermixed with silicon particles with increasing cycle number (up to 100 cycles). Conversely, the electrode cycled in EC/DEC/FEC is covered with a dense and uniform SEI and the silicon particle integrity is preserved which was hypothesized by Xu et al.[6] Here for the first time we present a comparative study to directly visualize the effects of FEC on SEI morphology in the first few cycles (1, 5 cycles) using STEM-EELS. Surprisingly, the same phenomenon was not observed after 100 cycles for the electrode cycled in EC/DEC/FEC. The SEI has similar morphology properties to the electrode cycled in EC/DEC, which is also consistent with the HIM images, previously mentioned.

The EELS spectra from the lithiated Si cycled in EC/DEC and EC/DEC/FEC after 1 cycle are compared with the possible reference compounds resulting from the electrolyte decomposition including LiF, Li_2CO_3, and Li_2O (**Figure 7**).[27,30] A comparison of the Li-K, C-K, O-K, and F-K edges taken from SEI cycled with EC/DEC indicate that the SEI mainly contains Li_2CO_3, which is due to EC reduction. However, the electrodes cycled in EC/DEC/FEC mainly contains LiF according to Li-K and F-K edge fine structures (Figure 7a,d). This is formed as a result of the FEC decomposition and salt dissolution which decomposes at a much higher voltage than that of EC/DEC,

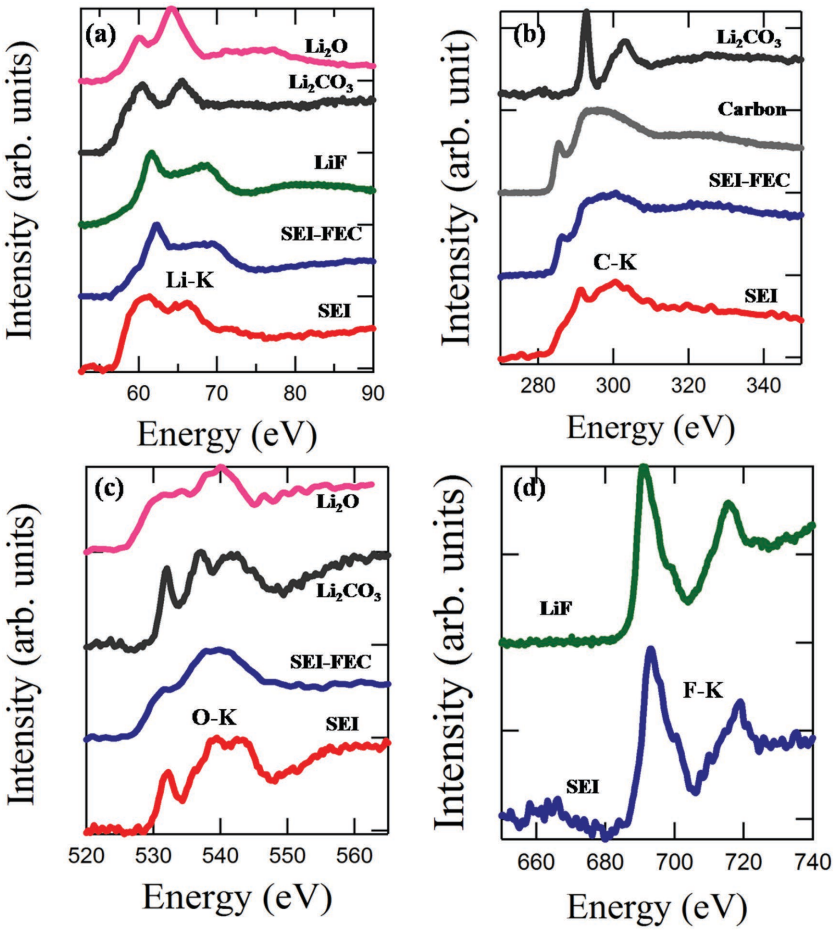

Figure 7. Comparison of SEI layer EELS fine structure in the lithiated Si after 1 cycle with reference compounds for a) Li K-edge, b) C-K edge, c) O-K edge, and d) F-K edge. SEI for the electrode cycled in EC/DEC shown in red (SEI) and electrode cycled in EC/DEC/FEC shown in blue (SEI-FEC).

therefore, limiting the degradation of EC/DEC which is consistent with previous results.[7,29] Figure 7a compares where the Li-K edges of the SEI generated by EC/DEC and EC/DEC/FEC. The SEI generated by adding of FEC shows the formation of Li_2O, which can occur when the electrolyte reacts with the SEI. Based on our EELS results, we did not observe SEI chemical changes for the electrodes with EC/DEC and EC/DEC/FEC after prolonged cycling (up to 100 cycles). These results are in agreement with the previous results.[6,31] It is necessary to note that in spite of using the low electron dose, electron beam damage may still preclude the detection of low content organic and inorganic compounds. As such, a surface sensitive XPS technique was utilized to further understand the SEI chemistry changes upon cycling for the electrodes cycled in EC/DEC and EC/DEC/FEC.

2.2.1. XPS Data Supporting EELS Data

Figure 8 demonstrates the relative composition of the first 10 nm of the SEI of electrodes cycled with (a,c,e) EC/DEC and (b,d,f) EC/DEC/FEC. The XPS analysis was performed after the (a,b) first lithiation, first delithiation, and (e,f) 100 cycles in the delithiated state.

The special resolution and detection limit of STEM/EELS make it difficult to determine the atomic composition of the parasitic electrolyte decomposition products over a large area. Given that EELS is a local technique, XPS was used as a complementary surface characterization technique to obtain a better understanding of the SEI using a large area scan (300 × 700 µm). Post hoc and ex situ XPS was used to avoid any environmental contamination by water vapor or oxygen which can alter the SEI composition, as demonstrated by Schroder et al.[20] and our previous work.[7] By studying the SEI composition via anoxic and anhydrous XPS, we can gain insights as to how EC/DEC/FEC affect the cycling performance of composite, avoiding any contamination.

The highly stable Si composite electrodes cycled with both electrolytes generated an SEI by galvanostatic electrochemical cycling. The XPS assignments follow a meticulous self-consistent fitting model previously used for Si anode types (shown in the supporting information).[32] Figure 8 shows a bar graph demonstrating the relative compositions of the SEI for electrodes cycled with EC/DEC and EC/DEC/FEC deduced from the XPS peak fittings (Figures S3–S7, Supporting Information). The inelastic mean free path of the photoexcited electrons limits the detection depth to 10 nm; therefore, Figure 8 demonstrates the outer most surface composition of the SEI generated by two electrolyte types. In our previous work, amorphous Si thin films (without binder or conductive additives) were used to clarify the FEC reduction mechanism and determine how FEC improves the SEI in the initial cycles,[7] however, this study focuses on determining the SEI morphology and chemical composition of the SEI in a composite electrode, which is how an Si electrode would be used in a real battery configuration. The previous model system study was used to decipher the convoluted SEI generated by a composite electrode because the binder and conductive additive contribute to the rapid SEI formation.

The atomic percentage of all the electrodes investigated is shown in Figure 8. Organic species are labeled C sp^3 for aliphatic carbon and may include adventitious carbon, ROR for alkoxy groups (ethers), ROCO for carboxyl groups (carboxylates, esters), and RCO_3 for carbonic esters and ionic carbonate salts. Ionic carbonate salts are difficult to deconvolute by XPS because of their similar binding energies and functional group (Li_2CO_3, $ROCO_2Li$). Therefore, when discussing RCO_3 it is likely that both these reduction products are being detected. The high resolution XPS spectra and peak fittings can be found in the Figures S3–S7 in the Supporting Information. Inorganic species include lithium fluoride (LiF), fluoro-phosphoro-oxides

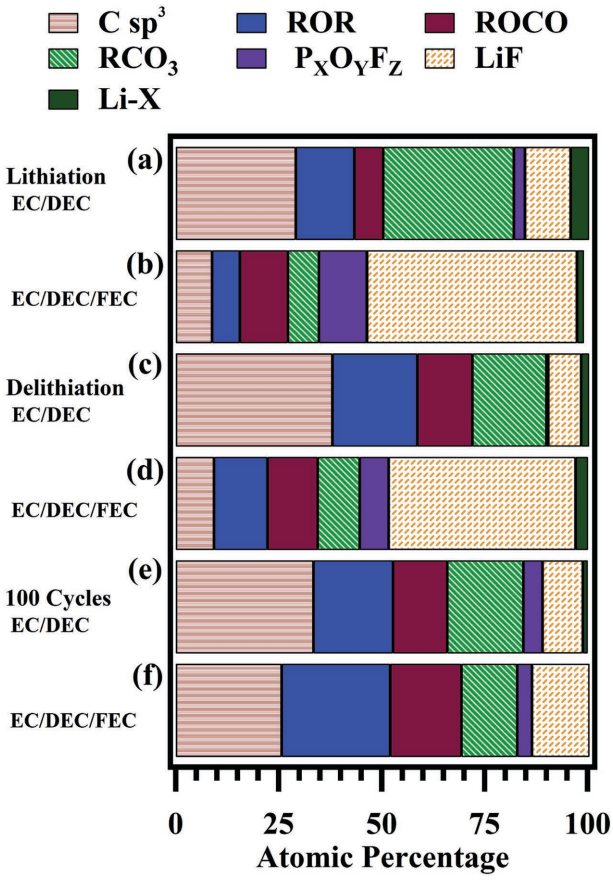

Figure 8. Relative composition of the SEI at Si NPs after a,b) first lithiation, c,d) first delithiation, and e,f) 100 cycles in the delithiated state.

($P_xO_yF_z$), and LiX (which could include alkyl lithium and lithium phosphoro-oxy-fluoride). Additionally, it is difficult to distinguish ionic lithium ions bound to organics such as carbonic esters and lithium alkoxides, also labeled LiX. As demonstrated, we observed little to no Si 2p signal for all cycled electrodes. Therefore, the SEI generated in the initial lithiation was much thicker than 10 nm given the Si 2p signal.

We propose that the variations in the SEI composition are explained by kinetics of the competing FEC versus EC reduction products perpetuated by the 60 nm Si particles. Though 60 nm crystalline Si particles help mitigate the volume expansion[5] (below the critical cracking limit), the surface area is increased which promotes the rapid SEI formation.[6,33–35] In the first lithiation step, we find the electrode cycled with EC/DEC contained ≈21.2% organic functionalities and the SEI formed by EC/DEC/FEC contained ≈18% organic functionalities. In our case, it is difficult to fully assign the C sp^3 carbon solely to SEI moieties because our electrode contains conductive carbon and binder which contribute to the signal as in our previous work.[7] Therefore, the atomic percentage of organic functionalities is solely based on ROR and ROCO species found in the SEI. The SEI comprised of 32% and 8% (atomic percent) carbonate species for the electrodes cycled with EC/DEC and EC/DEC/FEC, respectively making it difficult to properly quantify the organic SEI species. These results are consistent with the EELS data analysis, validating that the data is not the result of beam damage. Furthermore, the SEI generated from EC/DEC contains a higher concentration of ROCO and ROR (esters, ethers, carboxylates) 14.2% and 7%, respectively, where the electrode cycled with EC/DEC/FEC contains 6% ROR and 12% ROCO. Here, the formation of ROCO is more profound which may be attributed to the reduction mechanism of FEC while the electrode cycled with EC/DEC forms more ROR reduction products as a result of the EC and DEC decomposition. In the SEI generated by EC/DEC shows a higher concentration of RCO_3 functionalities (≈31%) while the SEI generated by EC/DEC/FEC has less (≈8%). This is due to the reduction potential and reaction kinetics, where FEC is more likely to form less carbonate based functionalities. It is widely accepted that FEC decomposes at higher reduction potential; therefore, the electrode cycled with EC/DEC/FEC contains 50% LiF whereas the electrode cycled with EC/DEC contains 12% LiF. Given that the EC/DEC electrolyte's only source of fluoride anion comes from the salt ($LiPF_6$), the indirect path of LiF formation through the reversible thermal decomposition of the salt (Reaction 2).[34,36,37] As a result, the electrode cycled with EC/DEC/FEC contains two reaction pathways to generate LiF. Furthermore, the high surface area of the 60 nm Si nanoparticles further increases decomposition kinetics of the SEI.[38] Here, we find no evidence of C—F bonds which is still a heavily disputed conclusion as a result of the FEC decomposition mechanism. However, determining the reduction mechanism of FEC is beyond the scope of this work because the analysis was carried out using a composite electrode containing binder and conductive additive which affect the SEI composition. Here, we are focusing on the morphology of the SEI over prolonged cycles using STEM and EELS and XPS is used to observe the chemical composition of the SEI to validate the EELS results.

In addition to LiF, the electrode cycled with EC/DEC/FEC contains more $P_xO_yF_z$ which is a function of multiple step reaction,[39] which form very stable oxides on the surface. These results are consistent with our previous study where the FEC containing electrolyte produced a higher concentration of $P_xO_yF_z$. Our findings are consistent with previous results, where the FEC containing electrolyte produces a more inorganic SEI in the initial lithiation (Equation (2)).

After delithiation, the SEI composition is consistent, where there is no major peak shift or appearance of new compounds (Supporting Information). However, the electrode cycled with EC/DEC contains less RCO_3 and more ROR and ROCO functionalities generating an SEI consisting of 92% atomic percent. The LiF and $P_xO_yF_z$ species form 8% of the total SEI consistent with the EELS results. The more organic species in the SEI forms a porous, "cloud" like SEI morphology. Therefore, more electrolyte decomposes as a result of the exposed Si surface that leads to poor electrochemical performance. Conversely, the electrode cycled with EC/DEC/FEC has little change in SEI composition (in terms of atomic percentage), where the LiF and $P_xO_yF_z$ species form ≈52% of the SEI composition. If we compare this percentage to the first lithiated percentage (≈70%), it demonstrates that the SEI formed is much more stable. Initially, EC/DEC/FEC forms a uniform dense coating (SEI) because of the fast reduction kinetics if FEC compared to EC.[40] Therefore, there is little change in the SEI composition in the first lithiated and delithiated state.

After 100 cycles, the SEI composition of both electrodes looks very similar which is consistent with the STEM images. The SEI formed from EC/DEC/FEC has more organic species than in the first cycle. There is a slightly more LiF and less RCO_3 moieties than the SEI generated from EC/DEC. Since there is only 10 wt% FEC additive and its rapid reduction kinetics in the first few cycles (even to 5 cycles), over prolonged cycles the FEC will eventually be depleted. This was first hypothesized in our previous work and is confirmed in this work. Therefore, LiF forms in the initial cycles forming a protective coating around the Si NP and after prolonged cycles the EC decomposition products dominate the SEI composition. As shown in the STEM images, after 100 cycles the SEI morphology is identical for both electrolytes, which is consistent with the XPS results. Furthermore, a more inorganic SEI is brittle and can crack easily, therefore, after prolonged cycling this layer will become mechanically unstable, exposing fresh Si surface forming a more organic SEI.

3. Conclusions

A comprehensive study of the effects of FEC on the Si electrochemical changes discovers new insights to the significance of SEI morphology and chemical changes that occur during electrochemical cycling using STEM/EELS analysis. Specifically, the direct visualization of SEI morphology evolution obtained for both electrode systems reveals that the electrode cycled in EC/DEC/FEC is covered with a uniform and stable SEI mainly for the first few cycles while the SEI of the electrode cycled in EC/DEC forms a porous and inhomogeneous SEI right away. The stable SEI formation can contribute to the improvement in electrochemical performance of Si NP electrode. Furthermore, according to the STEM-EELS profile results, less oxide layer (Li_xSiO_y) is found in the initial cycle on the Si electrode cycled with EC/DEC/FEC. Our XPS results provide a much larger length scale for the SEI chemical changes after cycling, which demonstrated that the electrode cycled in EC/DEC has a higher atomic percentage of Li_2CO_3 consistent with the EELS results. On the other hand, the electrode cycled in EC/DEC/FEC contained fewer carbonate species and more LiF, also correlating well with the STEM/EELS analysis. Thus, we propose two main reasons as the effects of FEC which result in the electrochemical improvements: (1), FEC decomposition products eliminate the Li_xSiO_y layer, and (2), the initial formation of homogeneous and dense SEI on the Si NPs. Therefore, the chemical composition formed with FEC additive is not the sole reason for improved capacity retention with cycling of Si electrode but the SEI density and morphology also plays a critical role in electrode stability. However, the mechanical property of such a dense SEI film may not be most ideal if large amount of lithiation/delithiation occurs upon long term cycling. Further investigation on how SEI morphology and composition changes with the degrees of lithiation/delithiation in the electrode cycled with EC/DEC/FEC can provide critical information for further improving and developing Si anodes as well as electrolyte additives.

4. Experimental Section

Battery Preparation and Electrochemical Cycling: Silicon electrodes were prepared by coating a slurry of silicon Nanopowder (NP) (average particle size of around 60 nm, Alfa Assar), Ketjenblack (Akzo Nobe: EC-600JD), and sodium carboxymethyl cellulose (degree of dubstitution = 0.9, M_w = 250 000, Sigma Aldrich) with a mass ratio of 2:1:1 onto thick rough copper foil (battery grade). First Si NP and KetjenBlack were ball milled for 20 min. The powder was added to a CMC water solution and placed in the homogenizer to mix. The slurry was casted on the Cu foil using a doctor-blading. The electrode was dried at 80 °C under vacuum for 12 h. The electrodes were punched and had a mass loading 0.5 mg of Si per cm^2. The coin cells were assembled in an argon-filled glovebox (Micromeritics ASAP 2010, H_2O < 0.1 ppm). The electrochemical half-cells were assembled using 2032 coin cells, polymer separators (Celgard), 1 mm thick lithium foil, 1 M $LiPF_6$ electrolyte solutions (battery grade, BASF) including traditional 1:1 (wt%) EC: DEC, and a blend of 45:45:10 (wt%) EC/DEC/FEC (fluoroethylene carbonate). The ≈100 uL of electrolyte was used in each cell. Half-cells were cycled in galvanostatic mode (0.05–1.0 V vs Li) at room temperature and a C/20 rate for the first cycle and a C/10 rate for all subsequent cycles on an Arbin battery cycler.

Surface Analysis-XPS: After electrochemical cycling, the cells were disassembled in the glovebox and washed with DEC to remove excess lithium salt. The washed electrodes were then transferred to the ultrahigh-vacuum environment using a reduced oxidation (RO_x) interface designed for transferring air-sensitive samples. The RO_x has methods and figures of merit to determine if the samples are ever exposed to additional traces of oxygen and water greater than those experienced in the glovebox environment, even during pump-down. The methods and components of the RO_x are described in further detail in the previous publication.[19] XPS was performed using a Kratos Ultra DLD XPS. Analysis followed similar methods used in previous work.[20,21] All XPS measurements were collected with a 300 μm by 700 μm spot size without using a charge neutralizer during acquisition. Survey scans were collected with a 1.0 eV resolution, followed by high-resolution 0.05 eV, 1 s scans of the carbon 1s, oxygen 1s, lithium 1s, silicon 2p, fluorine 1s, and phosphorus 2p regions.

Fits of the XPS spectra were performed with CasaXPS software (version 2.3.15, Casa Software Ltd.) to estimate the atomic compositions and chemical species comprising the SEI. All fitting followed a self-consistent method similar to the previous publication.[20,21] Spectral fits are shown in the Figures S3–S7 in the Supporting Information. All SEI species were assumed to be electronically insulating and were therefore fitted with linear backgrounds and with Voigt functions composed of 15% Lorentzian and 85% Gaussian following previous work.[22–27] Initial peak fits were made of the spectra using a Levenberg–Marquardt least-squares algorithm, and atoms in the same functionality were assumed to be stoichiometric. The resulting spectra were then refit and all spectra were shifted relative to the binding energy of the carbon 1s sp^3 oxidation state (assigned to 284.8 eV) to compensate for any charging during the measurement. The sum of the areas under the peaks were then used to determine relative composition of the outer-most ≈10 nm of the SEI.

HIM: Helium ion microscopy was performed using a Carl Zeiss Orion Plus System operating at 30 kV acceleration voltage and using 0.2–0.4 pA beam current. The base pressure in the analysis chamber was kept at 1×10^{-7} torr. No beam induced sample damage was observed.

STEM: The electrochemical cells were disassembled in an argon-filled glovebox, and the silicon electrodes were washed in DEC. The electrodes were then scraped to produce a fine powder and then placed on a TEM lacy carbon film supported on a copper grid. The TEM samples were loaded on a vacuum transfer holder and transferred to the TEM to avoid any contamination from air or water. ADF-STEM, and EELS were recorded at 197 kV with a JEOL-2010F microscope equipped with a Gatan-200 imaging filter spectrometer. The energy resolution of the EELS spectra measured from the full width at half magnitude of the zero-loss peak was 0.9 eV. In addition, a collection angle (β) of 20 mrad and a convergence angle (α) of 10 mrad were used for the acquisition of EELS spectra.

Supporting Information

Supporting Information is available from the Wiley Online Library or from the author.

Acknowledgements

This research was supported by the Office of Vehicle Technologies, U.S. Department of Energy under Contract No. DE-AC02-05CH11231, Subcontract No. 7073923 under the Advanced Battery Materials Research (BMR) Program. The Rutgers HIM is supported by NSF grant DMR-1126468. M.S. and J.A. contributed equally to this work. M.S. acknowledges Rutgers IAMDN and UCSD NCMIR for the use of electron microscopy facilities. J.A. would like to thank Dr. Hugo Celio and Dr. Anthony Dylla for their thoughtful discussions concerning these experiments. M.S. and J.A. would like to thank Emil Kim for the authorized use of table of contents figure. Y.S.M. would like to thank Ford URP program for partial support of her effort on this project.

Received: May 14, 2016
Revised: July 1, 2016
Published online:

[1] E. Markevich, G. Salitra, K. Fridman, R. Sharabi, G. Gershinsky, A. Garsuch, G. Semrau, M. A. Schmidt, D. Aurbach, *Langmuir* **2014**, *30*, 7414.
[2] N. Liu, H. Wu, M. T. McDowell, Y. Yao, C. Wang, Y. Cui, *Nano Lett.* **2012**, *12*, 3315.
[3] V. Etacheri, O. Haik, Y. Goffer, G. a. Roberts, I. C. Stefan, R. Fasching, D. Aurbach, *Langmuir* **2012**, *28*, 965.
[4] X. H. Liu, L. Zhong, S. Huang, S. X. Mao, T. Zhu, J. Y. Huang, *ACS Nano* **2012**, *6*, 1522.
[5] M. Gu, Y. Li, X. Li, S. Hu, X. Zhang, W. Xu, S. Thevuthasan, D. R. Baer, J.-G. Zhang, J. Liu, C. Wang, *ACS Nano* **2012**, *6*, 8439.
[6] C. Xu, F. Lindgren, B. Philippe, M. Gorgoi, F. Björefors, K. Edstrom, T. Gustafsson, *Chem. Mater.* **2015**, *27*, 2591.
[7] K. Schroder, J. Alvarado, T. A. Yersak, J. Li, N. Dudney, L. J. Webb, Y. S. Meng, K. J. Stevenson, *Chem. Mater.* **2015**, *27*, 5531.
[8] D. M. Piper, J. J. Travis, M. Young, S. Son, S. C. Kim, K. H. Oh, S. M. George, C. Ban, S. Lee, *Adv. Mater.* **2014**, *26*, 1596.
[9] M. Nie, B. L. Lucht, *J. Electrochem. Soc.* **2014**, *161*, A1001.
[10] L. Chen, K. Wang, X. Xie, J. Xie, *J. Power Sources* **2007**, *174*, 538.
[11] A. Magasinski, B. Zdyrko, I. Kovalenko, B. Hertzberg, R. Burtovyy, C. F. Huebner, T. F. Fuller, I. Luzinov, G. Yushin, *ACS Appl. Mater. Interfaces* **2010**, *2*, 3004.
[12] C. C. Nguyen, B. L. Lucht, *J. Electrochem. Soc.* **2014**, *161*, A1933.
[13] M. Nie, D. P. Abraham, Y. Chen, A. Bose, B. L. Lucht, *J. Phys. Chem. C* **2013**, *117*, 13403.
[14] H. Nakai, T. Kubota, A. Kita, A. Kawashima, *J. Electrochem. Soc.* **2011**, *158*, A798.
[15] M. Nie, D. Chalasani, D. P. Abraham, Y. Chen, A. Bose, B. L. Lucht, *J. Phys. Chem. C* **2013**, *117*, 1257.
[16] M. Sina, R. Thorpe, S. Rangan, N. Pereira, R. A. Bartynski, G. G. Amatucci, F. Cosandey, *J. Phys. Chem. C* **2015**, *119*, 9762.
[17] J. E. Owejan, J. P. Owejan, S. C. DeCaluwe, J. A. Dura, *Chem. Mater.* **2012**, *24*, 2133.
[18] N. Dupré, P. Moreau, E. De Vito, L. Quazuguel, M. Boniface, A. Bordes, C. Rudisch, P. Bayle-Guillemaud, D. Guyomard, *Chem. Mater.*, **2016**, *28*, 2557.
[19] C.-M. Park, J.-H. Kim, H. Kim, H.-J. Sohn, *Chem. Soc. Rev.* **2010**, *39*, 3115.
[20] K. W. Schroder, A. G. Dylla, S. J. Harris, L. J. Webb, K. J. Stevenson, *ACS Appl. Mater. Interfaces* **2014**, *6*, 21510.
[21] S. Dalavi, P. Guduru, B. L. Lucht, *J. Electrochem. Soc.* **2012**, *159*, A642.
[22] R. Egerton, *Micron* **2004**, *35*, 399.
[23] F. Lin, I. M. Markus, M. M. Doeff, H. L. Xin, *Sci. Rep.* **2014**, *4*, 5694.
[24] F. Cosandey, D. Su, M. Sina, N. Pereira, G. G. Amatucci, *Micron* **2012**, *43*, 22.
[25] A. Colder, F. Huisken, E. Trave, G. Ledoux, O. Guillois, C. Reynaud, H. Hofmeister, E. Pippel, *Nanotechnology* **2004**, *15*, L1.
[26] M. Gu, X.-C. Xiao, G. Liu, S. Thevuthasan, D. R. Baer, J.-G. Zhang, J. Liu, N. D. Browning, C.-M. Wang, *Sci. Rep.* **2014**, *4*, 3684.
[27] M. Sina, N. Pereira, G. G. Amatucci, F. Cosandey, *J. Phys. Chem. C* **2016**, *120*, 1337.
[28] K. Kimoto, T. Sekiguchi, T. Aoyama, *Jpn. Soc. Electron Microsc.* **1997**, *46*, 369.
[29] Y. He, D. M. Piper, M. Gu, J. J. Travis, S. M. George, S.-H. Lee, A. Genc, L. Pullan, J. Liu, S. X. Mao, J.-G. Zhang, C. Ban, C. Wang, *ACS Nano* **2014**, *8*, 11816.
[30] M. Sina, K.-W. Nam, D. Su, N. Pereira, X.-Q. Yang, G. G. Amatucci, F. Cosandey, *J. Mater. Chem. A* **2013**, *1*, 11629.
[31] C. Xu, F. Lindgren, B. Philippe, M. Gorgoi, F. Björefors, K. Edstrom, T. Gustafsson, C. Xu, F. Lindgren, B. Philippe, M. Gorgoi, F. Björefors, **2015**.
[32] K. W. Schroder, H. Celio, L. J. Webb, K. J. Stevenson, *J. Phys. Chem. C* **2012**, *116*, 19737.
[33] B. Philippe, R. Dedryvère, M. Gorgoi, H. Rensmo, D. Gonbeau, K. Edström, R. Dedryvere, K. Edstrom, *J. Am. Chem. Soc.* **2013**, *135*, 9829.
[34] B. Philippe, R. Dedryvère, M. Gorgoi, H. Rensmo, D. Gonbeau, K. Edström, *Chem. Mater.* **2013**, *25*, 394.
[35] B. Philippe, R. Dedryvère, J. Allouche, F. Lindgren, M. Gorgoi, H. Rensmo, D. Gonbeau, K. Edström, *Chem. Mater.* **2012**, *24*, 1107.
[36] O. S. Tasaki, S. J. Harris, *J. Phys. Chem. C* **2010**, *114*, 8076.
[37] P. Lu, C. Li, E. W. Schneider, S. J. Harris, *J. Phys. Chem. C* **2014**, *118*, 896.
[38] S. J. Harris, P. Lu, *J. Phys. Chem. C* **2013**, *117*, 6481.
[39] J. M. M. de la Hoz, P. B. Balbuena, *Phys. Chem. Chem. Phys.* **2014**, *16*, 17091.
[40] K. Leung, S. B. Rempe, M. E. Foster, Y. Ma, J. M. Martinez del la Hoz, N. Sai, P. B. Balbuena, J. M. M. del la Hoz, N. Sai, P. B. Balbuena, J. M. Martinez del la Hoz, N. Sai, P. B. Balbuena, *J. Electrochem. Soc.* **2014**, *161*, A213.